Mucosal tissue NK cells tune their function between optimal anti-pathogen activity and tissue protection

Sarah C. Vick[1], Eva Domenjo-Vila[1], Marie Frutoso[1,7], Raisa A. Glabman[2], Lakshmi S. Warrier[1,3], Sean M. Hughes[4], Anna C. Kirby[4], Michael F. Fialkow[4], Florian Hladik[1,4,5], Martin Prlic[1,3,6], Jennifer M. Lund[1,3]

[1]Vaccine and Infectious Disease Division, Fred Hutchinson Cancer Center, Seattle, WA, USA
[2]Comparative Pathology, Fred Hutchinson Cancer Center, Seattle, WA, USA
[3]Department of Global Health, University of Washington, Seattle, WA, USA
[4]Department of Obstetrics and Gynecology, University of Washington, Seattle, WA, USA
[5]Department of Medicine, University of Washington, Seattle, WA, USA
[6]Department of Immunology, University of Washington, Seattle, WA, USA
[7]Present address: UMR1227, LBAI, University Brest, Inserm, Brest, France

Corresponding authors: scvick@fredhutch.org, jlund@fredhutch.org

Abstract
Preserving barrier integrity is of great importance in mucosal tissues while simultaneously defending against inflammatory threats and exposures to pathogens. NK cells at barrier sites are essential for viral control during infections such as herpes simplex virus 2 (HSV-2) but must also balance pathogen response with tissue protection. We have characterized human tissue NK cells in the vaginal tissue (VT) as having distinct effector and tissue protective functions. Using scRNA-seq and high-parameter flow cytometry, we uncovered a unique signature for VT NK cells, indicating a reduced effector phenotype with increased factors related to tissue residency and immunoregulation at steady state. Despite their functionally quiescent nature, these cells were able to respond robustly to inflammatory signals, suggesting they are poised for pathogen response. We found that the gene signatures between mouse and human NK cells were remarkably similar, demonstrating the feasibility of using a mouse model to probe distinct NK cell functions during mucosal infection. In mice, VT NK cells responded robustly to acute HSV-2 infection and retained an enhanced recall potential after viral clearance. They also secreted tissue repair factors and played a role in restricting tissue damage following viral infection. Our data, using both human tissues and a mouse model, reveal an unexpected role of mucosal tissue NK cells in the VT in balancing host protection with tissue repair in the context of localized mucosal tissue infection.

Introduction
Mucosal surfaces are particularly vulnerable to infection as they are the site of many pathogen exposures. Furthermore, mucosal barrier surfaces have unique immune mechanisms to prevent infection while still maintaining tissue integrity. Immune populations important for direct cell killing and promoting inflammation, including CD8+ T cells and natural killer (NK) cells, work together to eliminate infections[1, 2]. NK cells

detect and eliminate virally infected cells through a combination of activating and inhibitory receptors[3], while T cells largely depend on antigen recognition to kill infected cells or pathogens. These cells both act through the secretion of pro-inflammatory cytokines like IFNg and direct killing of cells with molecules such as perforin and granzyme B. While the immune responses critical to protect the host from pathogens at barrier sites are starting to be well characterized, less is known about the resolution of inflammation after infection and the return to homeostasis. Immunoregulation at mucosal sites is important as excess inflammation can lead to tissue damage and thus compromised primary tissue function, so we sought to understand which cell populations are responsible for returning to homeostasis in mucosal sites.

NK cells are present in the circulation and within tissues. Tissue-resident NK cells have been described in multiple lymphoid and non-lymphoid sites, including the small intestines, lungs[4], salivary glands[5], liver[6, 7, 8], uterus[9, 10], and skin[11]. Tissue-resident NK cells differ from circulating NK cells in several ways, including expression of tissue retention markers[12] and reduced cytotoxicity[13, 14]. It is yet to be fully elucidated if tissue NK cells are transiently recruited from peripheral blood during inflammation[11, 15] or if tissue NK cells are developmentally distinct from circulating NK cells and constitute a long-lived, self-renewing tissue-resident population[4, 6, 12, 16, 17]. However, regardless of their ontogeny, the unique signatures of NK cells in mucosal and barrier tissue sites suggest unique functional capacities that require a thorough investigation in individual anatomic sites and disease contexts.

While characterization of NK cells in the VT is incomplete, it is known that NK cells play critical roles during host defense against sexually transmitted viral infections, such as human immunodeficiency virus (HIV)[18, 19]and herpes simplex virus 2 (HSV-2). During primary HSV-2 infection, NK cells provide a crucial early source of IFNg [20, 21]. Depletion of NK cells during primary HSV-2 infection in a mouse model leads to increased viral burden in vaginal tissue in addition to the spinal cord, demonstrating the role of NK cells in controlling infection[22]. In mice, it has been shown that memory-like NK cells are formed after genital HSV-2 infection[23], yet whether humans can also form memory-like NK cells after HSV-2 remains unknown.

While pro-inflammatory cytokines, including IFNg, are crucial for pathogen clearance, unrestrained NK cell responses, particularly at mucosal sites of virus infection, could lead to chronic immune activation and excess inflammation, thereby causing collateral tissue damage. Thus, mucosal NK cells may be a double-edged sword in the context of viral infection and we hypothesized that a balance between pathogen clearance and barrier homeostasis would be critical for overall host health. How this balance is maintained is unclear. Here, we characterize NK cells from human and murine VT and blood and demonstrate a transcriptional and protein signature for NK cells from VT. Our data indicates these cells are maintained in a quiescent state at homeostasis yet have the capacity to respond robustly to inflammatory signals. We additionally show that these VT NK cells can also secrete tissue repair factors that have a protective function after infection. With this finding, we identified a novel mechanism

whereby tissue NK cells mediate an active balance between anti-pathogen effector function and preservation and repair of host tissue health.

Results

scRNA-seq analysis reveals cell populations expressing tissue repair gene signatures enriched in vaginal tissue.

We performed single-cell RNA sequencing (scRNA-seq) on vaginal tissue (VT) and matched peripheral blood (PBMC) samples enriched for CD45+ immune cells from 4 healthy participants undergoing reconstructive vaginal surgery (Extended Data Figure 1A). We integrated the scRNA-seq data and calculated principal component analysis and Uniform Manifold Approximation and Projection (UMAP) for dimensionality reduction. We used SingleR to guide cell type recognition and manual cell annotation was confirmed by examining the top 8 differentially expressed genes across all clusters (Extended Data Figure 1B). We obtained approximately 32,000 cells and found most immune cell subsets represented in all donors including B cells, T cells, dendritic cells, monocytes, and natural killer (NK) cells (Figure 1A, Extended Data Figure 1C). CD8 and CD4 Effector/Memory T cells made up most of the immune cells from the VT and PBMC samples, while regulatory T cells, B cells, and NK cells also made up a substantial proportion of the immune cells from each donor (Extended Data Figure 1D). Immune cells from the VT and PBMC clustered separately (Figure 1B), suggesting that these populations may have different gene signatures, consistent with our previous work focused on vaginal tissue T cells [24, 25, 26].

To understand which cell populations participate in the balance of tissue homeostasis versus inflammatory immune response, we calculated the average expression of curated repair[27] and cytotoxic/effector gene signatures in our defined cell populations (Figure 1C). Blood effector/memory CD8 T cells and NK cells had the highest effector score of all the populations examined. In contrast, effector/memory CD8 T cells, regulatory T cells (Treg), and NK cell clusters from the VT were each enriched for a tissue repair gene signature (Figure 1C). Since the repair score was high specifically in immune cells isolated from the tissue, we analyzed the abundance of individual gene transcripts in immune cells in the VT and found that CD8 T cells and also NK cells score highly on both the effector and repair lists (Figure 1D). Unexpectedly, NK cells scored highly on the repair gene signature, suggesting that they could play a role in both inducing inflammation and restoring tissue integrity.

Tissue and circulating NK cells exhibit contrasting functional signatures.

The seeming dichotomy of circulating and tissue NK cells led us to further characterize the differences between these two populations. We confirmed the identity of the NK cell cluster as a discrete population based on expression of EOMES and lack of CD200R (Extended Data Figure 1E)[6, 28, 29, 30, 31]. Using published studies defining tissue NK cells [11, 12, 32], we compiled an NK cell phenotypic gene signature and compared blood NK cells to VT NK cells (Figure 2A). NK cells from VT were enriched for genes related to tissue residency and immune regulation, while transcripts related to effector and cytotoxic functions were decreased (Figure 2A). NK cells from the VT displayed an overall tissue resident signature compared to blood NK cells (Figure 2A). We then

performed differential gene expression analysis on NK cell clusters from PBMC compared to VT and identified 313 genes upregulated in VT NK cells compared to blood NK cells (Extended Figure 2A). To extend our findings from the transcript to the protein level, we utilized high-parameter flow cytometry to measure markers of NK cell activation, maturation, cytotoxicity, regulation, and tissue residency. Collagenase digestion has been shown to induce upregulation of genes associated with tissue residency[33] and so high parameter flow cytometry also allowed us to confirm our gene expression findings. We defined NK cells as CD45+, CD19-, CD14-, CD3-, NKp46+, as NKp46 was found previously to be a reliable marker for blood and tissue-derived NK cells (Extended Data Figure 2B)[34]. The NK cell population from the VT was overall enriched in gene transcripts related to tissue residency (RGS1, TCF7, CD69, and SELL) (Figure 2B). At the protein level, we measured well-characterized markers of tissue residency, CD69 and CD103 [4, 6, 8, 12, 35, 36, 37, 38, 39, 40, 41, 42] and TCF-1, which has been shown to regulate NK cell tissue residency differentiation and be necessary for tissue residency to occur[11]. These tissue resident markers were also expressed at a significantly higher frequency on NK cells from the VT (Figure 2C).

Many transcripts enriched in blood NK cells were related to cytotoxicity and effector function (GZMB, PRF1, FCGR3A, IFNG) and were minimally expressed in VT NK cells (Figure 2B). Accordingly, the frequency of NK cells expressing granzyme B was decreased in the VT compared to the blood (Figure 2C). In contrast, transcripts related to repair and immune regulation (TNFAIP3, AREG, TSC22D3, XCL2) were enriched in NK cell from the VT (Figure 2B). Examining NK cell maturation, the frequency of CD56brightCD16- NK cells was higher in the VT, while the frequency of CD56dimCD16+ NK was higher in the blood (Figure 2D). CD56bright NK cells predominate in the lymph nodes and at sites of inflammation, and these NK cells have been shown to have an immune regulatory function[43] through cytokine production[44]. Based on the increased frequency of CD56brightCD16- NK cells within the VT and our gene expression data, we hypothesized that NK cells in the VT would have a decreased maturation and activation phenotype at the protein level. The expression of activating and inhibitory receptors that regulate NK cell function (TIGIT, NKG2A, NKG2D) were increased on NK cells from the VT (Extended Data Figure 2C). We additionally measured markers of activation and maturation (CD57, CD11b, CD38) and saw the frequency of NK cells in the VT expressing these markers was significantly decreased when compared to the blood (Extended Data Figure 2C). CX3CR1 transcripts and protein were expressed almost exclusively in NK cells isolated from the blood and very minimally expressed on NK cells from the VT, whereas CXCR4 transcripts were expressed preferentially in NK cells from the VT (Extended Data Figure 2D).

In comparing NK cells from the blood to NK cells from the VT, we considered that we could be describing differences between the CD56brightCD16- and CD56dimCD16+ populations as these are differentially enriched in the two compartments. Using UMAP dimensionality reduction, we clustered just the NK cell populations from the PBMC and VT and identified CD16 *(FCGR3A)* negative NK cell populations both in PBMC and VT (Figure 2E). We then examined differentially expressed genes in CD16- NK cells and saw similar genes related to immune regulation and tissue repair upregulated in CD16-

NK cells from the VT (Figure 2F). This analysis suggests that NK cells from the VT are different than NK cells from the blood and present a less mature, more regulatory phenotype that may be poised to participate in immunoregulatory functions.

CD56^{bright} NK cells, found at high frequency in vaginal tissue, produce Amphiregulin.

In exploring factors promoting immune homeostasis and tissue protection in the VT, a finding from the scRNA-seq data indicated NK cells might be involved in tissue repair functions via expression of Amphiregulin (Areg) (Figure 1D, Figure 2B,2F). Areg is a key factor that promotes the restoration of tissue integrity following damage associated with inflammation[45, 46, 47]. We confirmed the transcriptional data by measuring Areg expression in NK cells by flow cytometry utilizing a fluorescence minus one (FMO) gating strategy to identify a true positive population (Extended Data Figure 3A). We found a significantly increased frequency of NK cells expressing Areg in tissue NK cells compared to the blood at steady-state (Figure 3A). Next, we wanted to determine which subset of NK cells was responsible for Areg production. Based on CD56 expression, we found that Areg was expressed by the CD56^{bright} population of NK cells from the VT (Figure 3B), similar to our finding that AREG expression was increased in the subset of vaginal CD16- NK cells compared to circulating CD16- NK cells (Figure 2F).

Next, we determined what factors induce Areg upregulation in NK cells. We hypothesized that NK cells might upregulate Areg under inflammatory conditions to balance inflammation with tissue protection. To test this hypothesis, we stimulated VT NK cells with IL-12 and IL-18, cytokines important for activating NK cells downstream of infection[48, 49, 50], for 24 hours and measured the frequency of Areg expression. We observed that exposure to activating cytokines did not significantly increase the frequency of NK cells expressing Areg in the VT (Figure 3C). We next tested additional combinations of IL-12, IL-18, IL-15, and IL-33 using blood NK cells[51]. We confirmed that Areg expression in circulating NK cells was largely restricted to the CD56^{bright} population (Figure 3D and Extended Data Figure 3C). The frequency of NK cells expressing Areg was significantly increased in cells stimulated with IL-33 alone and IL-18 alone. The combination of IL-18 and IL-33 together did not lead to a synergistic increase in Areg expression (Figure 3D). Combinations of IL-12, IL-15, and IL-18 did not significantly increase Areg expression (Figure 3D). To determine if Areg-producing NK cells in the VT were different to effector NK cells we looked for NK cells with double expression of IFNg or granzyme B alongside Areg after stimulation with IL-12/IL-18. We found that Areg production was not specific to either IFNg+ or IFNg- NK cell subsets, with similar findings for granzyme B (Extended Data Figure 3D). However, Areg+ NK cells were almost exclusively CD25+ (Extended Data Figure 3D), suggesting that Areg expression may be regulated by a more complex activation status than effector function alone.

NK cells from vaginal tissue are poised to respond robustly to stimulation.

We next wanted to investigate the anti-microbial function of NK cells in the VT. As this is an important mucosal barrier site, we hypothesized that local immune cells would need to be able to respond quickly to infection or inflammation. However, our data suggested a functionally quiescent profile of NK cells from the healthy VT at steady state. To mimic

induction of inflammation, we stimulated the cells with IL-12 and IL-18 for 24 hours[48, 49, 50]. This stimulation caused a higher frequency of vaginal NK cells to express the effector molecules granzyme B and IFNg (Figure 4A) as well as the upregulation of activation markers CD25 and CD69 (Figure 4A). In addition, we found that NK cells from the vaginal tissue expressed higher amounts of IFNg per cell as measured by median fluorescent intensity compared to blood NK cells (Figure 4B). These data suggest that although the NK cells in the vaginal tissue are relatively quiescent compared to their blood counterparts at steady state (Figure 2A-B), they are able to respond robustly to stimulation. Finally, markers of tissue residency, immune regulation, and effector function/maturation on NK cells after stimulation, including CD69, ICOS, and CD25, were increased in NK cells from both tissue sites after stimulation (Figure 4D). TCF-1 and NKG2D were decreased in NK cells from the VT after stimulation, while expression in NK cells from the blood remained consistent (Figure 4D). Expression of granzyme B in NK cells from the blood was high at baseline and was not significantly increased after stimulation (Figure 4D). These data indicate that the functionally quiescent nature of the NK cells from the VT is not due to inherent functional deficiencies, as the NK cells can respond robustly to stimulation, but rather suggests a mechanism of regulation to maintain reduced effector function in the mucosal tissue at homeostasis. We hypothesized that this tuning of tissue NK cells to be effector-like or produce tissue repair factors is crucial to maintaining barrier integrity in mucosal tissue.

Mouse NK cells recapitulate human tissue-specific NK cell phenotype.
To mechanistically define the factors that regulate the balance of NK cell inflammatory response with tissue repair in a setting of in vivo infection, we moved to a well-characterized mouse model of intravaginal herpes simplex virus 2 (HSV-2) infection[52]. To confirm the feasibility of using a mouse model to study NK cells in the VT, we first sorted NK1.1+ NK cells from blood and VT of naïve C57BL/6 mice and performed bulk RNA-seq. Comparing gene expression from VT NK cells and blood NK cells in mice revealed many DEGs (Extended Data Figure 4A) similar to those found in our human dataset (Extended Data Figure 2A). In addition, we confirmed our mouse gene expression data by examining protein expression by flow cytometry. To distinguish true tissue-resident NK cells from those merely in circulation, we utilized an intravenous (IV) antibody to label all cells in circulation before VT harvest. This allowed us to analyze NK cells from the VT that were IV label negative and, therefore, resident in the tissue (Extended Data Figure 4B). In mouse NK cells, the markers CD11b and CD27 distinguish stages of NK cell maturation similar to CD16 and CD56 in humans[53, 54, 55]. $CD11b^{-}CD27^{+}$ NK cells are a more immature subset with cytokine secreting potential[54]. This population was significantly more abundant in the VT compared to the blood (Figure 5A). In addition, we saw $CD11b^{+}CD27^{+}$ and $CD11b^{+}CD27^{-}$ NK cells with increased cytotoxic potential[53, 55, 56] were significantly higher in the blood compared to the VT (Figure 5A). This led us to hypothesize that similarly to NK cells from the VT in humans, mouse VT NK cells would be immunoregulatory and have increased tissue residency markers.

When we examined the signature of VT NK cells from mice, we found a similar pattern to the human data in that genes responsible for tissue residency *Cd69*, *Tcf7*,

and *Rgs1* were expressed at higher levels in NK cells from VT compared to the blood (Figure 5B). Concordantly, the frequency of NK cells from the VT expressing CD69 and TCF-1 was significantly increased compared to NK cells from the blood (Figure 5B). Genes related to NK cell maturation and activation *Ly6c2*, *Klrg1*, and *Itgam*[57, 58, 59] were expressed at lower levels in VT NK cells compared to blood, which was also confirmed by flow cytometry data (Figure 5A-B). We additionally found higher expression of immune regulation and tissue repair genes *Areg*, *Xcl1*, and *Tnfaip3* expressed in NK cells from VT (Figure 5B). Genes related to NK cell effector function *Gzma*, *Gzmb*, and *Prf1* were expressed at higher levels in blood NK cells compared to VT (Extended Data Figure 4C). CXCR4 was expressed significantly more in NK cells from the VT (Extended Data Figure 4C-D). Despite having lower transcripts, NK cells from the VT expressed CX3CR1 at higher levels than NK cells from the blood (Extended Data Figure 4C-D). Additionally, the frequency of NK cells expressing markers related to tissue retention and immune regulation CD49a, NKG2D, and CD103 were all significantly increased in the VT (Extended Data Figure 4D).

These findings supported those from our human dataset, confirming that both murine and human NK cells from the tissue have a gene signature that suggests less effector function and increased tissue residency and immune regulation at homeostasis. To confirm NK cells from our mouse model were consistent with NK cells from our human samples, we calculated a z-score of gene expression using the cluster average transcript data from human blood and VT NK cells and the bulk RNA-seq data from mouse blood and VT NK cells and compared genes important for NK cell function (Figure 5C). We found that the gene signatures between mouse and human NK cells were remarkably similar, demonstrating the feasibility of using a mouse model of HSV-2 infection to explore NK cell phenotypes upon mucosal infection and inflammation. Overall, this flow cytometry and gene expression data from mouse NK cells mirror human vaginal NK cells in having decreased cytotoxicity and increased tissue retention and immune regulation potential.

NK cells produce cytotoxic and tissue repair molecules during HSV-2 infection. To determine how tissue NK cells alter their function during mucosal infection to balance pathogen response with tissue repair, we examined NK cells in the VT at an acute and post-infection time point after localized vaginal HSV-2 infection. Mice were synchronized in the diestrous phase using Depo-Provera[52] and then inoculated 7 days later intravaginally with $2x10^6$ PFU of HSV-2 strain 186Kpn TK-[60] (Figure 6A). The TK^- mutant of HSV-2 resolves within 7 days without neurologic disease or death in C57BL/6 mice, allowing us to examine an acute time point with peak viral titers, 2 days post-infection (dpi), and after the viral infection has resolved and tissue repair is needed, 10dpi (Figure 6A). To determine how the transcriptional landscape of NK cells is altered throughout the course of infection, we performed bulk RNA-Seq on sorted NK cells from VT at day 0 (uninfected), 2dpi, and 10dpi. Principal component analysis (PCA) of the transcriptional data showed that NK cells from 2dpi clustered separately from NK cells isolated at 10dpi and from uninfected mice based on PC1 (Extended Data Figure 5A). NK cells from uninfected mice and 10dpi clustered separately based on PC2. This suggests that NK cells from uninfected mice and mice 10dpi are more similar

than NK cells from mice 2dpi. This was confirmed by differentially expressed gene (DEG) analysis (Extended Data Figure 5B). Specifically, there were 472 significant DEGs with an adjusted p-value less than 0.05 comparing NK cells from uninfected VT to 2dpi, indicating a large transcriptional change. Similarly, there were 505 significant DEGs between 2dpi and 10dpi. However, there were only 11 significant DEGs between uninfected and 10 dpi, suggesting that these populations of cells are more closely related, yet not identical (Extended Data Figure 5B-C).

Specific genes expressed by NK cells at 10 dpi indicated a tissue repair phenotype. Included in the genes unique to NK cells from 10dpi compared to uninfected are *Icos* and *Ly6c2*. Ly6C is thought to be a memory marker on tissue-resident NK cells after viral infection[61, 62], thereby potentially suggesting that vaginal NK cells retain enhanced functional capacity following mucosal infection with HSV-2. Additional evidence for induction of an NK cell memory-like population after infection came from upregulation of genes that classify adaptive NK cell populations, such as CD3 chain transcripts and members of the histocompatibility gene family, at 10dpi compared to uninfected. We saw genes that define this population reach significance when we reduced the stringency of our adjusted p-value cutoff to 0.1 (Extended Data Figure 5C). To examine the recall potential of NK cells post infection, we harvested VT at 2 dpi (acute) and 10 dpi (post-infection) (Figure 6A), stimulated the NK cells ex vivo with IL-12/IL-18 to mimic re-exposure to inflammation, and performed flow cytometry. There was a significant peak in the frequency of NK cells producing granzyme B at 2dpi, with a decrease to homeostatic levels by 10dpi (Figure 6B). We saw a similar pattern for IFNg production, though IFNg remained somewhat elevated at 10dpi, suggesting heightened recall potential of NK cells post infection (Figure 6B). We next wanted to confirm Ly6C protein expression as this could potentially suggest a memory-like NK cell population. We saw a significant increase in the frequency of NK cells expressing Ly6C at 10dpi compared to NK cells from uninfected mice (Figure 6B).

We next wanted to examine the tissue repair potential of NK cells during HSV-2 infection by measuring Areg expression. At homeostatic conditions in uninfected mice, NK cells isolated from the VT express significantly higher levels of Areg than NK cells from the blood (Figure 6C). When we measured Areg expression on NK cells at 2dpi (acute phase) or 10dpi (post HSV-2 clearance), we saw a peak of Areg-expressing NK cells 2dpi, with a return to homeostatic expression by 10dpi (Figure 6D). To determine if similar cues induce Areg by murine NK cells as in humans, splenocytes from uninfected mice were stimulated with combinations of IL-12, IL-15, IL-18, and IL-33, as we did for humans (Figure 3E). We saw that, as in humans, IL-18 and IL-33 together significantly increased the frequency of Areg+ NK cells over media alone (Figure 6E). Thus, NK cells may start producing Areg in response to inflammatory cues produced during peak infection to aid in subsequent tissue repair.

NK cell depletion after HSV-2 infection leads to increased tissue damage.
Finally, to test our hypothesis that NK cells play a unique role in tissue repair in the VT, separate from their role in pathogen clearance, we utilized our intravaginal infection model of HSV-2 and depleted NK cells after the infection was beginning to resolve, and

then looked at vaginal tissue pathology at 10dpi. Because NK cells are known to be important for the control of HSV-2 infection[63], we wanted to inguish the known role of NK cells in viral clearance early post-infection from their potential role in tissue repair later after infection. Based on the viral titers during HSV-2 TK- (Figure 6A), 2dpi is the peak of viral infection, with titers beginning to resolve quickly after 4dpi. Thus, we injected mice with anti-NK1.1 antibody (Ab) to deplete NK cells systemically or IgG2a isotype control Ab on 4dpi, 5dpi, and 8dpi. We then harvested VT at 10dpi for pathology scoring (Figure 7A). NK cell depletion was confirmed in both blood and VT using flow cytometry (Extended Data Figure 6A-B). VT were stained for H&E and scored by a blinded veterinary pathologist in four lesion categories which included vaginal epithelium, vaginal lamina propria, vaginal muscularis, and vaginal lumen, and received a score of 0-4 for each category (Figure 7B). VT depleted of NK cells after acute HSV-2 infection had significantly increased epithelial damage and lymphocyte infiltration compared to VT from isotype control mice (Figure 7C). The increased pathology occurred despite equal viral clearance: there were no differences in the viral load of vaginal washes between NK cell depleted and isotype control mice (Figure 7D). To test our hypothesis that Areg produced by NK cells could be leading to increased tissue repair after infection, we measured the total immune cell population (CD45+) expressing Areg in the VT of both groups by flow cytometry. We saw a decrease in Areg-expressing CD45+ cells in the NK cell depleted mice compared to the isotype control group (Figure 7E). A large frequency of total CD45+ immune cells expressed Areg as determined by the FMO (Extended Data Figure 6C), which was decreased after NK cell depletion (Figure 7F). This data supports that NK cells are a significant source of Areg in the VT during HSV-2 infection. Our data reveal an unexpected role of mucosal tissue NK cells in the VT in balancing host protection with tissue repair in context of localized mucosal tissue infection.

Discussion

For many infections, the mucosal barrier is the portal of pathogen exposure, yet the regulation of mucosal immunity is poorly understood. NK cells at mucosal sites are well-known to be critical for controlling infections. We show here that they unexpectedly also play a role in protecting this barrier site from immunopathology related tissue damage. In this study, we profile NK cells from the vaginal tissue of both humans and mice and find a unique phenotype for NK cells at this important barrier site that suggests a unique and previously unexplored functional capacity.

To the best of our knowledge, this is the first study demonstrating that NK cells have a tissue-resident signature in the VT. In comparing tissue-resident NK cells from the VT to other tissues, we observe several similarities but also some key differences. Dogra et al. examined human tissue-resident NK cells from non-lymphoid tissues and reported that the lungs were enriched with $CD56^{dim}CD16^{+}$ NK cells at levels similar to what is found in the blood. These NK cells also expressed high levels of CD57. In contrast, in the VT, we see an enrichment of $CD56^{bright}CD16^{-}$ NK cells with reduced expression of CD57. Dogra et al. did find that in the gut, there was an increased frequency of $CD56^{bright}CD16^{-}$ NK cells, similar to what we find in the VT. They also found that $CD56^{bright}CD16^{-}$ NK cells were enriched for a tissue-resident gene signature with

significant CD69 and CD103 expression. This suggests that NK cells from different tissues may have different signatures, potentially depending on the tissue microenvironment or their function at these sites. Torcellan et al. examined tissue-resident NK cells in mice from the uterus and skin and found a high frequency of tissue-resident NK cells in the uterus at homeostasis, but very few in the skin. However, after infection, they saw an expansion of tissue-resident NK cells in the skin. Furthermore, they found a tissue-resident gene signature in skin NK cells after infection very similar to what we found in the VT with high expression of transcription factor Tcf7, which they found to be crucial for maintaining a tissue-resident phenotype.

NK cells have been well characterized in the uterus owing to their importance during pregnancy. As the VT and uterus are both components of the female genital tract (FGT), we were interested in comparing these two populations. One key difference between NK cells from these distinct FGT anatomical sites is that NK cells from the VT produce IFNg upon stimulation, whereas NK cells from the uterus have reduced IFNg production[64] and have a reduced capacity for cytotoxicity[13, 14]. This important difference most likely represents the different roles these NK cells play in the FGT compartments. While uterine NK cells in the upper FGT most likely play a large role in pregnancy, NK cells in the VT are likely to be more poised to respond to sexually-transmitted infection pathogens that represent a larger threat in the lower FGT. Furthermore, maintaining mucosal barrier integrity is likely to be of great importance in the vaginal canal, which faces inflammatory threats including dysbiosis of the vaginal flora, physical and inflammatory trauma from sexual intercourse, and exposure to pathogens.

One striking finding from our study was the production of Areg by human and murine NK cells (Figure 3 and Figure 6C-E) and the unexpected role of NK cells in tissue repair (Figure 7). While other immune cells have been shown to play an important role in the repair of tissue after infection, such as ILCs and T cells[65, 66, 67], this role has not been well elucidated for NK cells. The notion of NK cells as important for tissue integrity is supported by our data in which NK cell depletion after acute HSV-2 infection leads to increased tissue pathology (Figure 7). While it is known that NK cells are important during peak HSV-2 infection to manage viral control through production of IFNg[20, 21, 22], we have shown that NK cells are also necessary after viral clearance to aid in restoration of tissue integrity. There have been other reports in models of inflammation that suggest NK cell depletion leads to increased epithelial damage and inflammation. Liu et al. demonstrate that in a model of corneal epithelial abrasion, NK cells modulate the inflammatory response in the eye and support wound healing. In their model, NK cell depletion led to an increased number of neutrophils in the wound and reduced epithelial cell division, leading to overall delayed wound healing[68]. In a model of allergic airway inflammation, depletion of NK cells led to delayed clearance of airway eosinophils and CD4 T-cells, leading to disruption of airway resolution[69]. It is possible that in addition to aiding in tissue repair through Areg production, NK cells also play an immunoregulatory function by the suppression of T cells in the VT. NK cells can regulate antiviral immune responses by direct elimination of activated CD4 T cells, thereby reducing inflammation in the tissue[70, 71]. We show that NK cell depletion after acute

HSV-2 infection leads to increased immune infiltration in the tissue (Figure 7B-C), which could be due to unrestrained T cell proliferation.

A limitation of the study is that the HSV-2 status of human tissue donors in the study is unknown, and so the study of vaginal tissue NK cells in the context of infection is limited to the study of a mouse model. Because a mouse model of HSV-2 has some key differences from human HSV-2 infection, future studies will involve recruiting women with known HSV-2 serostatus and active viral shedding and lesions to longitudinally evaluate NK cell cytotoxic and tissue protective capacity as we have done for T cells[72]. Nevertheless, we demonstrate that murine vaginal NK cells share a signature with human vaginal NK cells (Figure 5C), thereby highlighting the applicability of our studies of mouse VT NK cells in the context of human HSV-2 infection.

Additionally, a key area of research moving forward will be to further explore the mechanism whereby NK cells balance the anti-pathogen response with tissue protection and repair. Studies in T cells have demonstrated Tregs are able to produce Areg after IL-33/IL-18 stimulation[65], while memory CD8 T cell populations require TCR stimulation for Areg production[66]. We demonstrate that in NK cells, IL-33 and IL-18 together induce Areg in human and mouse NK cell populations (Figure 3D and Figure 6E), suggesting that there may be unique signals that tune the tissue NK cell response between an anti-pathogen, cytotoxic profile and a tissue healing profile. IL-33 and IL-18 are both members of the IL-1 family and are produced in response to inflammation and HSV-2 infection[73, 74, 75, 76, 77, 78, 79]. A major unanswered question is if there is a tissue-specific signal allowing for this balance of function. Future studies will explore the dynamics of cytokine signaling during infection that promotes the dual nature of NK cell function to transition from protection from pathogens to tissue protection.

Here, we characterize circulating and vaginal tissue NK cells from human and mouse and demonstrate a transcriptional and protein signature for NK cells from VT. These tissue NK cells are maintained in a functionally quiescent profile at steady state yet are poised to respond robustly to inflammatory signals from tissue infection. We additionally show that these VT NK cells can secrete the tissue repair factor Amphiregulin, which could have a protective function after resolution of infection. We propose a novel mechanism whereby tissue NK cells mediate an active balance between anti-pathogen effector function and preservation of host tissue integrity. Thus, mucosal NK cells are a double-edged sword in the context of viral infection and provide a balance between pathogen clearance and barrier homeostasis.

Methods

Human Tissue Collection and Processing

Human blood and VT were collected from women undergoing vaginal reconstructive surgeries for pelvic organ prolapse. Any samples suspected of malignancy were excluded from collection. All participants signed a written informed consent prior to inclusion in the study, and the protocols were approved by the institutional review board at the Fred Hutchinson Cancer Center and the University of Washington (IRB 4323). Blood was collected into sodium heparin tubes (BD Vacutainer) and mixed. Blood was

diluted 1:2 in PBS, layered on a Lymphoprep (StemCell Technologies) gradient and centrifuged at 1200 rpm for 20 min. The PBMC layer was then removed and washed with PBS. Tissues were transported from the clinic in ice cold PBS and immediately processed upon arrival (within 1–2 h of removal). Vaginal tissues were trimmed to 2 mm of epithelium and the outermost stroma. Tissue was minced and pipetted into a 50mL Falcon tube with 30 mL of digestion medium and shaken for 30. Minutes at 37 °C. Digestion medium consisted of collagenase II (700 units/ml, Sigma-Aldrich) and DNAse I (1 unit/ml, Sigma-Aldrich) in a 1:1 mixture of PBS and R15 as previously described[80]. The sample was then aspirated and expelled from a 30 mL syringe through a 16-gauge blunt needle and strained through a 70-um strainer. This process was repeated with the remaining tissue pieces and then cells were pelleted and resuspended in fresh RP10 medium.

Human Cell Culture

Directly following isolation or thawing, cells were cultured with recombinant human IL-12 (Preprotech) at 10ng/mL and recombinant human IL-18 (Peprotech) at 10ng/mL for 24 hours in RP10 at 37ºC and 5% CO2. Brefeldin A was added in the last 4 hours of culture. For some experiments, cells were cultured in IL-12 (10ng/mL), IL-18 (10ng/mL), IL-15 (50ng/mL, Peprotech), or IL-33 (50ng/mL, R&D Systems) in RP10 containing 50ng/mL IL-2 (Peprotech) and cultured for 5 days at 37ºC and 5% CO2.

Flow Cytometry

For flow cytometric analysis good practices were followed as outlined in the guidelines for use of flow cytometry[81] and consensus suggestions for data analysis[82]. Directly following isolation or thawing, cells were incubated with Fc-blocking reagent (BioLegend Trustain FcX) and fixable UV Blue Live/Dead reagent (ThermoFisher) in PBS (Gibco) for 20 min at room temperature. After this, cells were incubated for 20 min at room temperature with 50 µl total volume of antibody master mix freshly prepared in Brilliant staining buffer (BD Biosciences), followed by two washes in fluorescence-activated cell sorting (FACS) buffer (PBS with 0.5% FBS). All antibodies were titrated and used at optimal dilution, and staining procedures were performed in 96-well round-bottom plates. The stained cells were fixed with eBioscience Foxp3 Transcription Factor Fixation/Permeabilization Kit (Thermo Fisher) for 30 min at room temperature, the stained for intracellular (IFNg, granzyme B (GzmB), or Areg) or intranuclear staining (Ki67 or TCF1) in 50 µl total volume of antibody master mix for 30 min. Samples were stored at 4ºC in the dark until run on flow cytometer. Single-stained controls were prepared with every experiment using antibody capture beads (OneComp eBeads, Thermo Fisher) diluted in FACS buffer, or ArC Amine Reactive Compensation beads (Thermo Fisher) for Live/Dead reagent. All single stain controls were treated the same as the samples (including fixation procedures).

All samples were acquired using a FACSymphony A5 (BD Biosciences) and FACSDiva acquisition software (BD Biosciences). Detector voltages were optimized using a modified voltage titration approach[83] and standardized from day to day using MFI target values and 6-peak Ultra Rainbow Beads[84] (Spherotec). After acquisition, data was exported in FCS 3.1 format and analyzed using FlowJo (version 10.6.x, and 10.7.x, BD

Biosciences). Samples were analyzed using manual gating with doublets being excluded by FSC-A vs FSC-H gating. Gates were kept the same across all samples except where changes in the density distribution of populations clearly indicated the need for sample-specific adjustment.

Single-cell RNA-Seq

Single-cell RNA-seq was performed on sort-purified CD45+ and NKp46+ NK cells derived from either cryopreserved blood or VT tissue samples. In total, 8 samples were sequenced from 4 donors.

Whole transcriptome single-cell library preparation and sequencing

Cryovials of PBMC and VT cells were thawed and added to prewarmed RP10 media and washed. VT cells were enriched for CD45+ cells (EasySep Release Human CD45 Positive Selection Kit, Stemcell) and all samples were stained with Live/Dead and FcBlock for 20 min at room temperature. Cells were resuspended in 80µl of antibody cocktail and 20µl Sample Tag and incubated for 20 min at room temperature. Cells were washed and resuspended in RP10. Cell sorting was performed on a FACSymphony S6 cell sorter (BD Biosciences) with a 70-µm nozzle at 70 psi sheath pressure into Eppendorf tubes with 300 µl RP10. Total CD45+ cells were sorted until around 90% of the desired number cell number was reached, and then NKp46+ cells were sorted until a total desired cell number was reached, or until sample end.

After sorting, cells were pooled, counted, and loaded onto a nano-well cartridge (BD Rhapsody), lysed inside the wells followed by mRNA capture on cell capture beads. Cell Capture Beads were retrieved and washed prior to performing reverse transcription and treatment with Exonuclease I. Libraries were prepared using mRNA whole transcriptome analysis and sample tag library preparation (BD Rhaspsody)[85]. Briefly, mRNA and Sample-Tag were amplified separately and purified using double-sided size selection using SPRIselect magnetic beads (Beckman Coulter). Quality of PCR products was determined by using an Agilent 2200 TapeStation with High Sensitivity D5000 ScreenTape (Agilent) in the Fred Hutch Genomics Shared Resource laboratory. The quantity of PCR products was determined by Qubit with Qubit 1x dsDNA HS Assay (Q33231). Final libraries were diluted to 4nM and multiplexed for paired-end sequencing on a NovaSeq 6000 (Illumina) using an S1 flow cell. For the mRNA library, we targeted 30,000 reads per cell, and for the Sample-Tag libraries, 1,200 reads per cell.

Pre-processing for whole transcriptome analysis (WTA) and Seurat workflow

Fastq files were processed via the standard Rhapsody analysis pipeline (BD Biosciences) on Seven Bridges (www.sevenbridges.com). In brief, after read filtering, reads are aligned to a reference genome and annotated, barcodes and UMIs are counted, followed by determining putative cells. The final output was analyzed in R using the package Seurat[86] (version 4.0), with scripts based on the following general guidelines for analysis of scRNA-seq data[87]. In brief, for whole-transcriptome data, only cells that had a valid Sample Tag, at least 200 genes and less than 35% mitochondrial genes were included in analysis. All acquired samples were merged into a single Seurat object, followed by a natural log normalization using a scale factor of 10,000,

determination of variable genes using the vst method, and a z-score scaling. Principal component analysis was used to generate 75 principal components and the first 25 were used to calculate UMAP, and graph-based clustering with a resolution of 0.5. For cell annotation, we applied SingleR as a purely data-driven approach[88], and used the expression of typical lineage transcripts to verify the cell label annotation.

For all differential gene expression analyses we utilized the Seurat implementation of MAST (model-based analysis of single-cell transcriptomes). For calculating the Repair scores we used the AddModuleScore function of Seurat. The genes used were as follows: Effector: GZMB, GZMA, PRF1, NKG7, FGFBP2, GNLY, TNF, IFNG; Repair: IL10RA, HIF1A, CD44, LYST, TNFAIP3, AREG, TSC22D3, TGFB1.

Mice

WT mice on a C57BL/6 background were used.

HSV-2 Infection and Viral Titers

HSV-2 186DeltaKpn TK- strain (HSV-2 TK)[89] was grown and titered on Vero cells. Mice were subcutaneously injected with 2 mg of medroxyprogesterone acetate (MDPA) injectable suspension (Depo-Provera) dissolved in sterile PBS 5–7 days before vaginal infection. For HSV-2 infection, mice were infected intravaginally with 10^6 PFU of HSV-2 TK-. To determine viral titers, vaginal washes were performed daily after infection with 50 µL titration buffer (PBS + 1% FBS + 1% Glucose + 0.01% MgCl + 0.01% CaCl). One mL of diluted vaginal washes were added to confluent flasks of Vero cells for 1 hour at 37°C, then human IgG at 4.8mg/ml was added to prevent further infection. Vero cells were incubated at 37ºC and 5% CO2 for 48 hours and then plaques were counted to determine plaque forming units per mL.

Mouse Tissue Collection and Processing

The vaginal tissue and cervix were harvested and minced thoroughly in prewarmed digestion medium, which was freshly prepared and consisted of DMEM, collagenase D (2 mg/mL; Sigma-Aldrich), 500 µL DNase (15 µg/mL), and 10% FBS. The minced tissue was incubated for 30 minutes at 37°C on a shaker. After incubation, the minced tissue was spun at 1200 rpm for 5 minutes. To prepare single-cell suspensions, 5 mL of HBSS/EDTA solution (2% FBS in HBSS without calcium and magnesium and 5 mM EDTA) was added to the pellet, and the mixture was homogenized through a 70 µm strainer. Blood was collected through cardiac puncture after euthanasia into Heparin in PBS. ACK lysis buffer was added to the blood for 15 minutes and centrifuged at 300 *g* for 5 minutes. The ACK-treated cells were suspended in HBSS/EDTA solution before proceeding with flow staining.

Mouse Cell Culture and Cell Depletion

Immune cells isolated from the VT or blood were cultured in round-bottom 96-well plates with 20ng/mL recombinant mouse IL-12 (BioLegend) and 10 ng/mL recombinant mouse IL-18 (BioLegend) in RP10 with BrefeldinA at 1:1000 dilution for 4 hours at 37ºC at 5% CO2. For some experiments, splenocytes were cultured in IL-12 (20ng/mL), IL-18

(10ng/mL), IL-15 (20ng/mL, Peprotech), or IL-33 (50ng/mL, R&D Systems) in RP10 containing 20ng/mL IL-2 (Peprotech) and cultured for 24 hours at 37ºC and 5% CO2. NK cells were depleted using InVivo anti-mouse NK1.1 clone PK136 (BioXCell). Anti-NK1.1 mAb or IgG2a Isotype Control mAb (BioXCell) were injected intraperitoneally at a concentration of 200ug in 200ul on days 4, 5, and 9 after HSV-2 TK- infection.

Bulk RNA-seq

Bulk RNA-seq was performed on 250 sort-purified NK1.1+ NK cells derived from either blood or VT tissue samples harvested from uninfected mice or from mice infected with HSV-2 TK- on days 2 and 10 post-infection. In total, 24 samples were sequenced, and each condition was represented by 4 biological replicates.

Cell sorting was performed on a Sony MA900 (Sony) using a 100-µm sorting chip with 90% sort efficiency and 90-95% purity. Cells were sorted directly into reaction buffer from the SMART-Seq v4 Ultra Low Input RNA Kit for Sequencing (Takara), and reverse transcription was performed followed by PCR amplification to generate full-length amplified cDNA. Bulk RNA-seq was performed by the Genomics Core at Benaroya Research Institute. Sequencing libraries were constructed using the NexteraXT DNA sample preparation kit with unique dual indexes (Illumina) to generate Illumina-compatible barcoded libraries. Libraries were pooled and quantified using a Qubit® Fluorometer (Life Technologies). Sequencing of pooled libraries was carried out on a NextSeq 2000 sequencer (Illumina) with paired-end 59-base reads (Illumina) with a target depth of 5 million reads per sample. Base calls were processed to FASTQs on BaseSpace (Illumina), and a base call quality-trimming step was applied to remove low-confidence base calls from the ends of reads. The FASTQs were aligned to the GRCm38 mouse reference genome, using STAR v.2.4.2a and gene counts were generated using htseq-count. QC and metrics analysis was performed using the Picard family of tools (v1.134). Filtered and normalized gene counts were generated from the raw counts by trimmed-mean of M values (TMM) normalization and filtered for genes that are expressed with at least 1 count per million total reads in at least 10% of the total number of libraries. To detect differentially expressed genes between sorted cell subsets, the RNA-seq analysis functionality of the linear models for microarray data (Limma) R package was used[90, 91, 92]. Expression counts were normalized using the TMM algorithm[93]. A false discovery rate adjustment was applied to correct for multiple testing.

H&E & Whole Slide Digital Imaging

Hematoxylin and Eosin (H&E) staining and whole slide digital imaging was performed by the Fred Hutchinson Cancer Center Experimental Histopathology Shared Resource (P30 CA015704). Tissues were formalin-fixed and paraffin embedded on an automated tissue processor (Sakura Tissue-Tek VIP), sectioned at 4-5 um onto charged slides, baked at 60°C, stained using an automated stainer (Sakura Tissue-Tek Prisma) for H&E staining and cover slipped with permanent mounting media. Whole slide digital imaging was performed on an Olympus VS200 at 20X.

Histopathology Scoring

Slides were examined by a board-certified veterinary pathologist. Digital slides were annotated to exclude cervical, uroepithelial and uterine tissue from grading. Each vaginal tract was examined in four lesion categories which included vaginal epithelium, vaginal lamina propria, vaginal muscularis, and vaginal lumen, and received a score of 0-4 for each category. *Vaginal Epithelium* Score 0: No lesions, Score 1: Epithelial surface is multifocally tattered, rare leukocytes and/or neutrophils within the epithelium, Score 2: Clusters of neutrophils within the epithelium, Score 3: Epithelium is thin and eroded, Score 4: Epithelium is ulcerated; *Vaginal Lamina Propria and Vaginal Muscularis* Score 0: No lesions, Score 1: Rare neutrophils and/or leukocytes, Score 2: Small clusters of neutrophils and/or leukocytes, Score 3: Multifocal clusters of neutrophils and/or leukocytes beginning to coalesce and/or forming follicles, Score 4: leukocytes arranged in sheets; *Vaginal Lumen* Score 0: No lesions, Score 1: Rare cellular debris in lumen, Score 2: <10% of vaginal lumen contains cellular debris, Score 3: 10-25% of vaginal lumen contains cellular debris, Score 4: >25% of vaginal lumen contains cellular debris.

Acknowledgments
We thank all members of the Lund and Prlic labs for their helpful discussions on experimental findings and manuscript preparation throughout this process. This work was supported by the following grants from the National Institutes of Health: R01 AI131914 (to JML), R01 AI141435 (to JML), R01 AI172111 (to FH and JML) and R01 HD114505 (to JML). SCV was supported by T32 AI007509 and K99 AI180649-02. LSW was supported by T32 AI083203. This research was supported by the Experimental Histopathology Shared Resource, RRID:SCR_022612 and Comparative Pathology Shared Resource RRID:SCR_022610 of the Fred Hutch/University of Washington/Seattle Children's Cancer Consortium (P30 CA015704).

References

1. Sun, J.C. & Lanier, L.L. NK cell development, homeostasis and function: parallels with CD8(+) T cells. *Nat Rev Immunol* **11**, 645-657 (2011).

2. Cook, K.D., Waggoner, S.N. & Whitmire, J.K. NK cells and their ability to modulate T cells during virus infections. *Crit Rev Immunol* **34**, 359-388 (2014).

3. Lanier, L.L. Evolutionary struggles between NK cells and viruses. *Nat Rev Immunol* **8**, 259-268 (2008).

4. Marquardt, N. *et al.* Unique transcriptional and protein-expression signature in human lung tissue-resident NK cells. *Nat Commun* **10**, 3841 (2019).

5. Gasteiger, G., Fan, X., Dikiy, S., Lee, S.Y. & Rudensky, A.Y. Tissue residency of innate lymphoid cells in lymphoid and nonlymphoid organs. *Science* **350**, 981-985 (2015).

6. Sojka, D.K. *et al.* Tissue-resident natural killer (NK) cells are cell lineages distinct from thymic and conventional splenic NK cells. *Elife* **3**, e01659 (2014).

7. Peng, H. *et al.* Liver-resident NK cells confer adaptive immunity in skin-contact inflammation. *J Clin Invest* **123**, 1444-1456 (2013).

8. Hudspeth, K. *et al.* Human liver-resident CD56(bright)/CD16(neg) NK cells are retained within hepatic sinusoids via the engagement of CCR5 and CXCR6 pathways. *J Autoimmun* **66**, 40-50 (2016).

9. Male, V. & Moffett, A. Natural Killer Cells in the Human Uterine Mucosa. *Annu Rev Immunol* **41**, 127-151 (2023).

10. Dogra, P. & Farber, D.L. Stealth Killing by Uterine NK Cells for Tolerance and Tissue Homeostasis. *Cell* **182**, 1074-1076 (2020).

11. Torcellan, T. *et al.* Circulating NK cells establish tissue residency upon acute infection of skin and mediate accelerated effector responses to secondary infection. *Immunity* **57**, 124-140 e127 (2024).

12. Dogra, P. *et al.* Tissue Determinants of Human NK Cell Development, Function, and Residence. *Cell* **180**, 749-763 e713 (2020).

13. Ritson, A. & Bulmer, J.N. Isolation and functional studies of granulated lymphocytes in first trimester human decidua. *Clin Exp Immunol* **77**, 263-268 (1989).

14. Ferry, B.L. *et al.* Cell populations in the human early pregnancy decidua: natural killer activity and response to interleukin-2 of CD56-positive large granular lymphocytes. *Immunology* **70**, 446-452 (1990).

15. Zimmer, C.L. *et al.* NK cells are activated and primed for skin-homing during acute dengue virus infection in humans. *Nat Commun* **10**, 3897 (2019).

16. Cortez, V.S. *et al.* Transforming Growth Factor-beta Signaling Guides the Differentiation of Innate Lymphoid Cells in Salivary Glands. *Immunity* **44**, 1127-1139 (2016).

17. Sojka, D.K., Yang, L. & Yokoyama, W.M. Uterine Natural Killer Cells. *Front Immunol* **10**, 960 (2019).

18. Quillay, H. *et al.* NK cells control HIV-1 infection of macrophages through soluble factors and cellular contacts in the human decidua. *Retrovirology* **13**, 39 (2016).

19. Oliva, A. *et al.* Natural killer cells from human immunodeficiency virus (HIV)-infected individuals are an important source of CC-chemokines and suppress HIV-1 entry and replication in vitro. *J Clin Invest* **102**, 223-231 (1998).

20. Ashkar, A.A. & Rosenthal, K.L. Interleukin-15 and natural killer and NKT cells play a critical role in innate protection against genital herpes simplex virus type 2 infection. *J Virol* **77**, 10168-10171 (2003).

21. Lee, A.J. *et al.* Inflammatory monocytes require type I interferon receptor signaling to activate NK cells via IL-18 during a mucosal viral infection. *J Exp Med* **214**, 1153-1167 (2017).

22. Thapa, M., Kuziel, W.A. & Carr, D.J. Susceptibility of CCR5-deficient mice to genital herpes simplex virus type 2 is linked to NK cell mobilization. *J Virol* **81**, 3704-3713 (2007).

23. Abdul-Careem, M.F. *et al.* Genital HSV-2 infection induces short-term NK cell memory. *PLoS One* **7**, e32821 (2012).

24. Pattacini, L. *et al.* A pro-inflammatory CD8+ T-cell subset patrols the cervicovaginal tract. *Mucosal Immunol* **12**, 1118-1129 (2019).

25. Traxinger, B. *et al.* Mucosal viral infection induces a regulatory T cell activation phenotype distinct from tissue residency in mouse and human tissues. *Mucosal Immunol* **15**, 1012-1027 (2022).

26. Woodward Davis, A.S. *et al.* The human memory T cell compartment changes across tissues of the female reproductive tract. *Mucosal Immunol* **14**, 862-872 (2021).

27. Haberman, Y. *et al.* Mucosal Inflammatory and Wound Healing Gene Programs Reveal Targets for Stricturing Behavior in Pediatric Crohn's Disease. *J Crohns Colitis* **15**, 273-286 (2020).

28. Klose, C.S.N. *et al.* Differentiation of type 1 ILCs from a common progenitor to all helper-like innate lymphoid cell lineages. *Cell* **157**, 340-356 (2014).

29. Daussy, C. *et al.* T-bet and Eomes instruct the development of two distinct natural killer cell lineages in the liver and in the bone marrow. *J Exp Med* **211**, 563-577 (2014).

30. Gordon, S.M. *et al.* The transcription factors T-bet and Eomes control key checkpoints of natural killer cell maturation. *Immunity* **36**, 55-67 (2012).

31. Nagasawa, M. *et al.* Correction: KLRG1 and NKp46 discriminate subpopulations of human CD117(+)CRTH2(-) ILCs biased toward ILC2 or ILC3. *J Exp Med* **216**, 2221-2222 (2019).

32. Lopes, N. *et al.* Tissue-specific transcriptional profiles and heterogeneity of natural killer cells and group 1 innate lymphoid cells. *Cell Rep Med* **3**, 100812 (2022).

33. Crowl, J.T. *et al.* Tissue-resident memory CD8(+) T cells possess unique transcriptional, epigenetic and functional adaptations to different tissue environments. *Nat Immunol* **23**, 1121-1131 (2022).

34. Frutoso, M., Mair, F. & Prlic, M. OMIP-070: NKp46-Based 27-Color Phenotyping to Define Natural Killer Cells Isolated From Human Tumor Tissues. *Cytometry A* **97**, 1052-1056 (2020).

35. Mackay, L.K. *et al.* Cutting edge: CD69 interference with sphingosine-1-phosphate receptor function regulates peripheral T cell retention. *J Immunol* **194**, 2059-2063 (2015).

36. Freud, A.G. *et al.* A human CD34(+) subset resides in lymph nodes and differentiates into CD56bright natural killer cells. *Immunity* **22**, 295-304 (2005).

37. Gaynor, L.M. & Colucci, F. Uterine Natural Killer Cells: Functional Distinctions and Influence on Pregnancy in Humans and Mice. *Front Immunol* **8**, 467 (2017).

38. Geissmann, F. *et al.* Intravascular immune surveillance by CXCR6+ NKT cells patrolling liver sinusoids. *PLoS Biol* **3**, e113 (2005).

39. Melsen, J.E. *et al.* Human Bone Marrow-Resident Natural Killer Cells Have a Unique Transcriptional Profile and Resemble Resident Memory CD8(+) T Cells. *Front Immunol* **9**, 1829 (2018).

40. Montaldo, E. *et al.* Unique Eomes(+) NK Cell Subsets Are Present in Uterus and Decidua During Early Pregnancy. *Front Immunol* **6**, 646 (2015).

41. Shi, F.D., Ljunggren, H.G., La Cava, A. & Van Kaer, L. Organ-specific features of natural killer cells. *Nat Rev Immunol* **11**, 658-671 (2011).

42. Victorino, F. *et al.* Tissue-Resident NK Cells Mediate Ischemic Kidney Injury and Are Not Depleted by Anti-Asialo-GM1 Antibody. *J Immunol* **195**, 4973-4985 (2015).

43. Cooper, M.A. *et al.* Human natural killer cells: a unique innate immunoregulatory role for the CD56(bright) subset. *Blood* **97**, 3146-3151 (2001).

44. Carson, W.E., Fehniger, T.A. & Caligiuri, M.A. CD56bright natural killer cell subsets: characterization of distinct functional responses to interleukin-2 and the c-kit ligand. *Eur J Immunol* **27**, 354-360 (1997).

45. Burzyn, D. *et al.* A special population of regulatory T cells potentiates muscle repair. *Cell* **155**, 1282-1295 (2013).

46. Jamieson, A.M. *et al.* Role of tissue protection in lethal respiratory viral-bacterial coinfection. *Science* **340**, 1230-1234 (2013).

47. Monticelli, L.A. *et al.* Innate lymphoid cells promote lung-tissue homeostasis after infection with influenza virus. *Nat Immunol* **12**, 1045-1054 (2011).

48. Chaix, J. *et al.* Cutting edge: Priming of NK cells by IL-18. *J Immunol* **181**, 1627-1631 (2008).

49. Chan, S.H. *et al.* Induction of interferon gamma production by natural killer cell stimulatory factor: characterization of the responder cells and synergy with other inducers. *J Exp Med* **173**, 869-879 (1991).

50. Hunter, C.A., Gabriel, K.E., Radzanowski, T., Neyer, L.E. & Remington, J.S. Type I interferons enhance production of IFN-gamma by NK cells. *Immunol Lett* **59**, 1-5 (1997).

51. Wang, Y. *et al.* Transcriptional and chromatin profiling of human blood innate lymphoid cell subsets sheds light on HIV-1 pathogenesis. *EMBO J* **42**, e114153 (2023).

52. Linehan, M.M. *et al.* In vivo role of nectin-1 in entry of herpes simplex virus type 1 (HSV-1) and HSV-2 through the vaginal mucosa. *J Virol* **78**, 2530-2536 (2004).

53. Chiossone, L. *et al.* Maturation of mouse NK cells is a 4-stage developmental program. *Blood* **113**, 5488-5496 (2009).

54. Fu, B. *et al.* CD11b and CD27 reflect distinct population and functional specialization in human natural killer cells. *Immunology* **133**, 350-359 (2011).

55. Hayakawa, Y., Huntington, N.D., Nutt, S.L. & Smyth, M.J. Functional subsets of mouse natural killer cells. *Immunol Rev* **214**, 47-55 (2006).

56. Kim, S. *et al.* In vivo developmental stages in murine natural killer cell maturation. *Nat Immunol* **3**, 523-528 (2002).

57. Huntington, N.D. *et al.* NK cell maturation and peripheral homeostasis is associated with KLRG1 up-regulation. *J Immunol* **178**, 4764-4770 (2007).

58. Omi, A., Enomoto, Y., Kiniwa, T., Miyata, N. & Miyajima, A. Mature resting Ly6C(high) natural killer cells can be reactivated by IL-15. *Eur J Immunol* **44**, 2638-2647 (2014).

59. Robbins, S.H., Tessmer, M.S., Mikayama, T. & Brossay, L. Expansion and contraction of the NK cell compartment in response to murine cytomegalovirus infection. *J Immunol* **173**, 259-266 (2004).

60. Stroop, W.G., Banks, M.C., Qavi, H., Chodosh, J. & Brown, S.M. A thymidine kinase deficient HSV-2 strain causes acute keratitis and establishes trigeminal ganglionic latency, but poorly reactivates in vivo. *J Med Virol* **43**, 297-309 (1994).

61. Riggan, L. *et al.* The transcription factor Fli1 restricts the formation of memory precursor NK cells during viral infection. *Nat Immunol* **23**, 556-567 (2022).

62. Schuster, I.S. *et al.* Infection induces tissue-resident memory NK cells that safeguard tissue health. *Immunity* **56**, 531-546 e536 (2023).

63. Milligan, G.N. & Bernstein, D.I. Interferon-gamma enhances resolution of herpes simplex virus type 2 infection of the murine genital tract. *Virology* **229**, 259-268 (1997).

64. Saito, S. *et al.* The effect of interleukin 2 and transforming growth factor-beta 2 (TGF-beta 2) on the proliferation and natural killer activity of decidual CD16-CD56bright natural killer cells. *Cell Immunol* **152**, 605-613 (1993).

65. Arpaia, N. *et al.* A Distinct Function of Regulatory T Cells in Tissue Protection. *Cell* **162**, 1078-1089 (2015).

66. Delacher, M. *et al.* The effector program of human CD8 T cells supports tissue remodeling. *J Exp Med* **221** (2024).

67. Krishnan, S. *et al.* Amphiregulin-producing gammadelta T cells are vital for safeguarding oral barrier immune homeostasis. *Proc Natl Acad Sci U S A* **115**, 10738-10743 (2018).

68. Liu, Q., Smith, C.W., Zhang, W., Burns, A.R. & Li, Z. NK cells modulate the inflammatory response to corneal epithelial abrasion and thereby support wound healing. *Am J Pathol* **181**, 452-462 (2012).

69. Haworth, O., Cernadas, M. & Levy, B.D. NK cells are effectors for resolvin E1 in the timely resolution of allergic airway inflammation. *J Immunol* **186**, 6129-6135 (2011).

70. Rydyznski, C. *et al.* Generation of cellular immune memory and B-cell immunity is impaired by natural killer cells. *Nat Commun* **6**, 6375 (2015).

71. Waggoner, S.N., Cornberg, M., Selin, L.K. & Welsh, R.M. Natural killer cells act as rheostats modulating antiviral T cells. *Nature* **481**, 394-398 (2011).

72. Dave, V. *et al.* Recurrent infection transiently expands human tissue T cells while maintaining long-term homeostasis. *J Exp Med* **220** (2023).

73. Aoki, R. *et al.* Mast cells play a key role in host defense against herpes simplex virus infection through TNF-alpha and IL-6 production. *J Invest Dermatol* **133**, 2170-2179 (2013).

74. Arshad, M.I., Khan, H.A., Noel, G., Piquet-Pellorce, C. & Samson, M. Potential Therapeutic Aspects of Alarmin Cytokine Interleukin 33 or Its Inhibitors in Various Diseases. *Clin Ther* **38**, 1000-1016 e1001 (2016).

75. Cayrol, C. & Girard, J.P. IL-33: an alarmin cytokine with crucial roles in innate immunity, inflammation and allergy. *Curr Opin Immunol* **31**, 31-37 (2014).

76. Ingram, J.T., Yi, J.S. & Zajac, A.J. Exhausted CD8 T cells downregulate the IL-18 receptor and become unresponsive to inflammatory cytokines and bacterial co-infections. *PLoS Pathog* **7**, e1002273 (2011).

77. Liu, B. *et al.* Interleukin-18 improves the early defence system against influenza virus infection by augmenting natural killer cell-mediated cytotoxicity. *J Gen Virol* **85**, 423-428 (2004).

78. Molofsky, A.B. *et al.* Interleukin-33 and Interferon-gamma Counter-Regulate Group 2 Innate Lymphoid Cell Activation during Immune Perturbation. *Immunity* **43**, 161-174 (2015).

79. Zalinger, Z.B., Elliott, R. & Weiss, S.R. Role of the inflammasome-related cytokines Il-1 and Il-18 during infection with murine coronavirus. *J Neurovirol* **23**, 845-854 (2017).

80. McKinnon, L.R. *et al.* Optimizing viable leukocyte sampling from the female genital tract for clinical trials: an international multi-site study. *PLoS One* **9**, e85675 (2014).

81. Cossarizza, A. *et al.* Guidelines for the use of flow cytometry and cell sorting in immunological studies (third edition). *Eur J Immunol* **51**, 2708-3145 (2021).

82. Liechti, T. *et al.* An updated guide for the perplexed: cytometry in the high-dimensional era. *Nat Immunol* **22**, 1190-1197 (2021).

83. Perfetto, S.P., Ambrozak, D., Nguyen, R., Chattopadhyay, P.K. & Roederer, M. Quality assurance for polychromatic flow cytometry using a suite of calibration beads. *Nat Protoc* **7**, 2067-2079 (2012).

84. Mair, F. & Tyznik, A.J. High-Dimensional Immunophenotyping with Fluorescence-Based Cytometry: A Practical Guidebook. *Methods Mol Biol* **2032**, 1-29 (2019).

85. Erickson, J.R. *et al.* AbSeq Protocol Using the Nano-Well Cartridge-Based Rhapsody Platform to Generate Protein and Transcript Expression Data on the Single-Cell Level. *STAR Protoc* **1** (2020).

86. Butler, A., Hoffman, P., Smibert, P., Papalexi, E. & Satija, R. Integrating single-cell transcriptomic data across different conditions, technologies, and species. *Nat Biotechnol* **36**, 411-420 (2018).

87. Amezquita, R.A. *et al.* Publisher Correction: Orchestrating single-cell analysis with Bioconductor. *Nat Methods* **17**, 242 (2020).

88. Finak, G. *et al.* MAST: a flexible statistical framework for assessing transcriptional changes and characterizing heterogeneity in single-cell RNA sequencing data. *Genome Biol* **16**, 278 (2015).

89. Jones, C.A., Taylor, T.J. & Knipe, D.M. Biological properties of herpes simplex virus 2 replication-defective mutant strains in a murine nasal infection model. *Virology* **278**, 137-150 (2000).

90. Law, C.W., Chen, Y., Shi, W. & Smyth, G.K. voom: Precision weights unlock linear model analysis tools for RNA-seq read counts. *Genome Biol* **15**, R29 (2014).

91. Phipson, B., Lee, S., Majewski, I.J., Alexander, W.S. & Smyth, G.K. Robust Hyperparameter Estimation Protects against Hypervariable Genes and Improves Power to Detect Differential Expression. *Ann Appl Stat* **10**, 946-963 (2016).

92. Ritchie, M.E. *et al.* limma powers differential expression analyses for RNA-sequencing and microarray studies. *Nucleic Acids Res* **43**, e47 (2015).

93. Robinson, M.D. & Oshlack, A. A scaling normalization method for differential expression analysis of RNA-seq data. *Genome Biol* **11**, R25 (2010).

Figure 1.

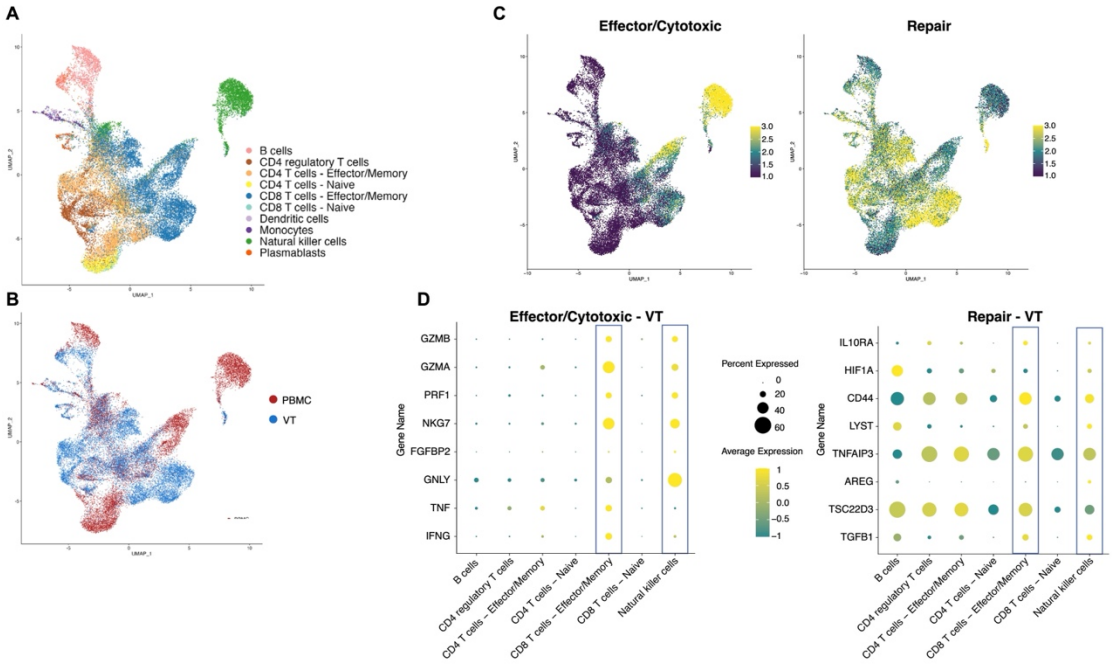

Figure 1. scRNA-seq analysis reveals vaginal tissue (VT) immune cell populations with repair gene signature. We performed single-cell RNA sequencing (scRNA-seq) on vaginal tissue (VT) and matching blood (PBMC) samples enriched for CD45+ immune cells from 4 healthy donors. Fastq files were processed via the standard Rhapsody analysis pipeline on Seven Bridges. After read filtering, reads were aligned to a reference genome and annotated, barcodes and UMIs were counted, followed by determining putative cells. The final output was analyzed in R using Seurat. Principal component analysis was performed to calculate UMAP and graph-based clustering with a resolution between 0.2 and 0.6. For cell annotation, we applied SingleR. **A**) UMAP plot colored by clustering based on transcripts. **B**) UMAP plot based on tissue type. **C**) UMAP plot showing enrichment of effector/cytotoxic or repair gene signature. **D**) Scaled dot plot showing average transcript expression (color) and percent expression (dot size) of transcripts of effector/cytotoxic and repair gene signatures for VT samples (n=4). In **A-C**, graphs show combined data for n = 4 for PBMC samples and n = 4 for VT samples.

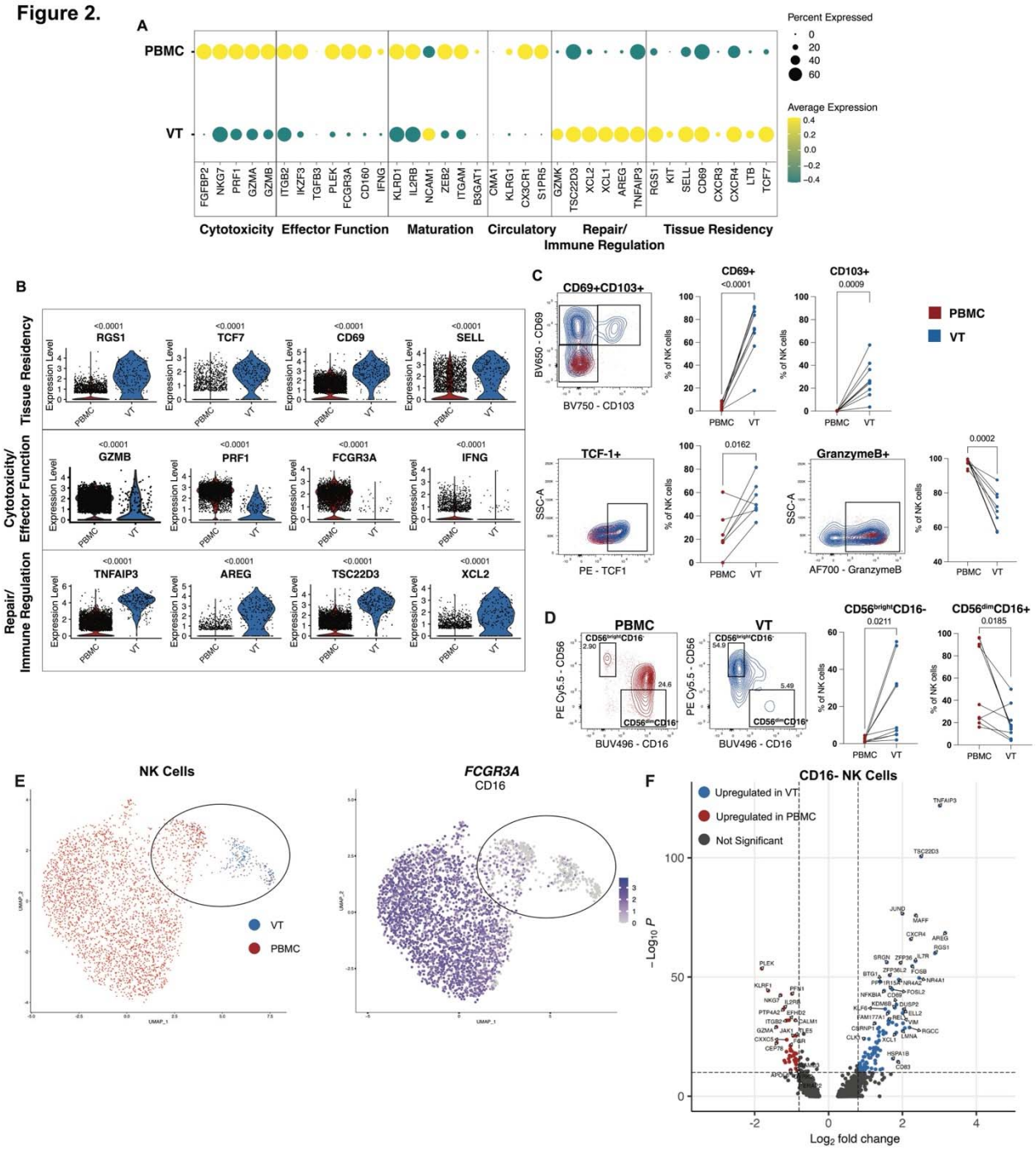

Figure 2. Tissue NK cells and circulating NK cells display differential phenotypic signatures at steady state. Single-cell RNA-seq or flow cytometry was performed on immune cells isolated from paired vaginal tissue (VT) or blood (PBMC) from healthy donors**. A**) Scaled dot plot showing average transcript expression (color) and percent expression (dot size) of select NK cell transcripts from PBMC cluster and VT cluster. **B**) Violin plots showing the expression of selected transcripts for the NK cell clusters from PBMC (left) and the VT (right). All graphs show combined data for n = 4 for PBMC

samples and n = 4 for VT samples. **C**) Example flow plot and graphed frequencies of NK cells expressing markers of tissue residency and cytotoxicity. CD69, CD103, and granzyme B show combined data for n = 10 for PBMC samples and n = 10 for VT samples. TCF-1 shows combined data for n=7 PBMC samples and n=7 VT samples. **D**) Example flow plots of CD56 and CD16 expression on NK cells from PBMCs (left) or VT (right). Graphs demonstrate frequencies of gated CD56 and CD16 populations. Lines indicate paired samples. All graphs show combined data for n = 10 for PBMC samples and n = 10 for VT samples. Statistical analyses were performed using paired t test, p values listed. **E**) UMAP plot based on PBMC and VT NK cell clusters overlaid with FCGR3A (CD16) expression. The black circle indicates populations used to calculate differentially expressed genes in F. **F**) Volcano plot showing differential gene expression of CD16- NK cell clusters from PBMC vs VT analyzed using the Seurat implementation of MAST (model-based analysis of single cell transcriptomes). Data for n = 4 for PBMC samples and n = 4 for VT samples.

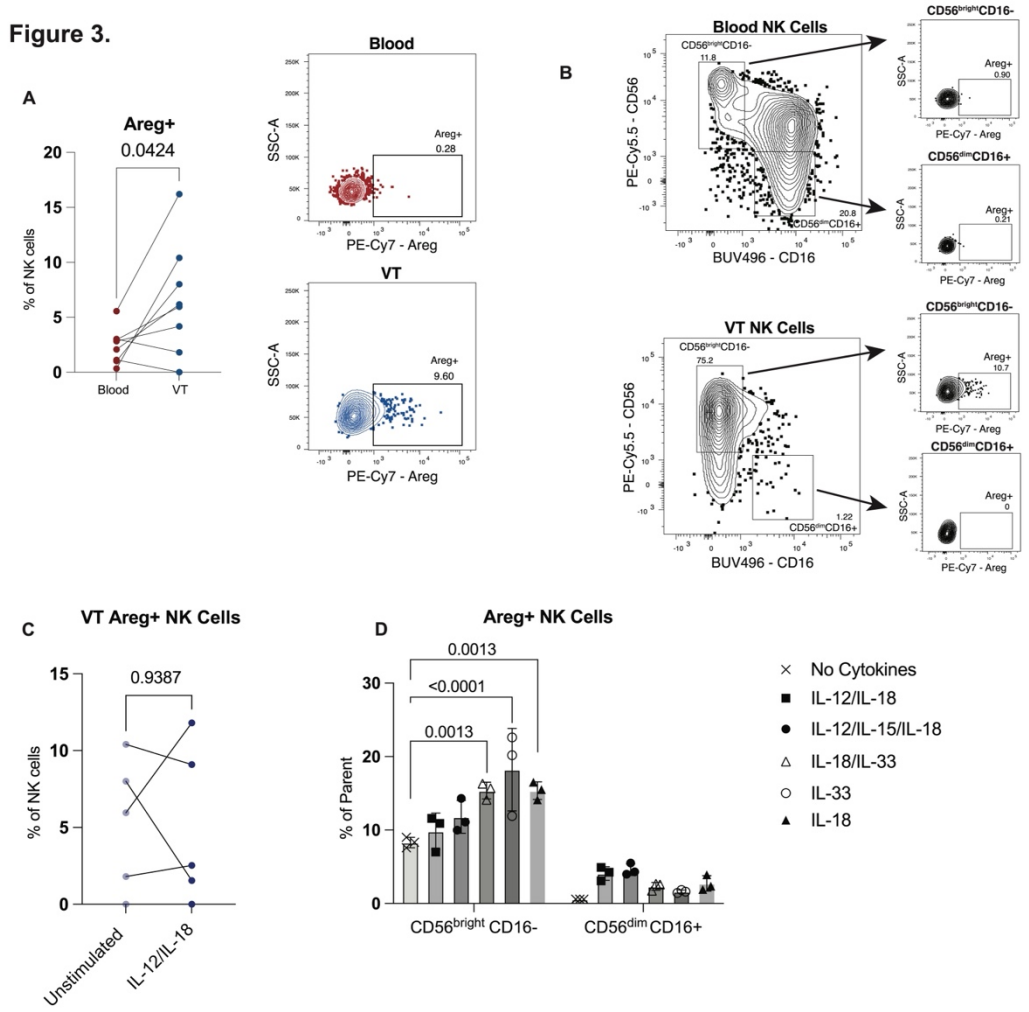

Figure 3. CD56^{bright} NK cells, found in high frequency in vaginal tissue, produce Amphiregulin. Flow cytometry was performed on immune cells isolated from vaginal tissue (VT) or blood (PBMC) from healthy donors. **A**) Paired graph and example flow plot demonstrate frequencies of NK cells expressing Amphiregulin (Areg) in blood (n=8) compared to VT (n=8). **B**) Representative flow plot of CD56^{bright}CD16^{-} or CD56^{dim}CD16^{+} NK cells expressing Areg. **C**) Paired graph demonstrates frequency of NK cells from VT expressing Areg after ex vivo stimulation for 24 hours unstimulated (n=5) or with IL-12/IL-18 (n=5). **D**) PBMCs were cultured in RP10 and IL-2 for 5 days with different cytokine stimulation conditions. The graphs indicate the frequency of Areg+ CD56^{bright}CD16^{-} or CD56^{dim}CD16^{+} NK cells. In **A** and **C**, statistical analyses were performed using paired t test, p values listed. In **D**, data are presented as mean with SD, and statistical analysis used 2way ANOVA, p values listed when significant.

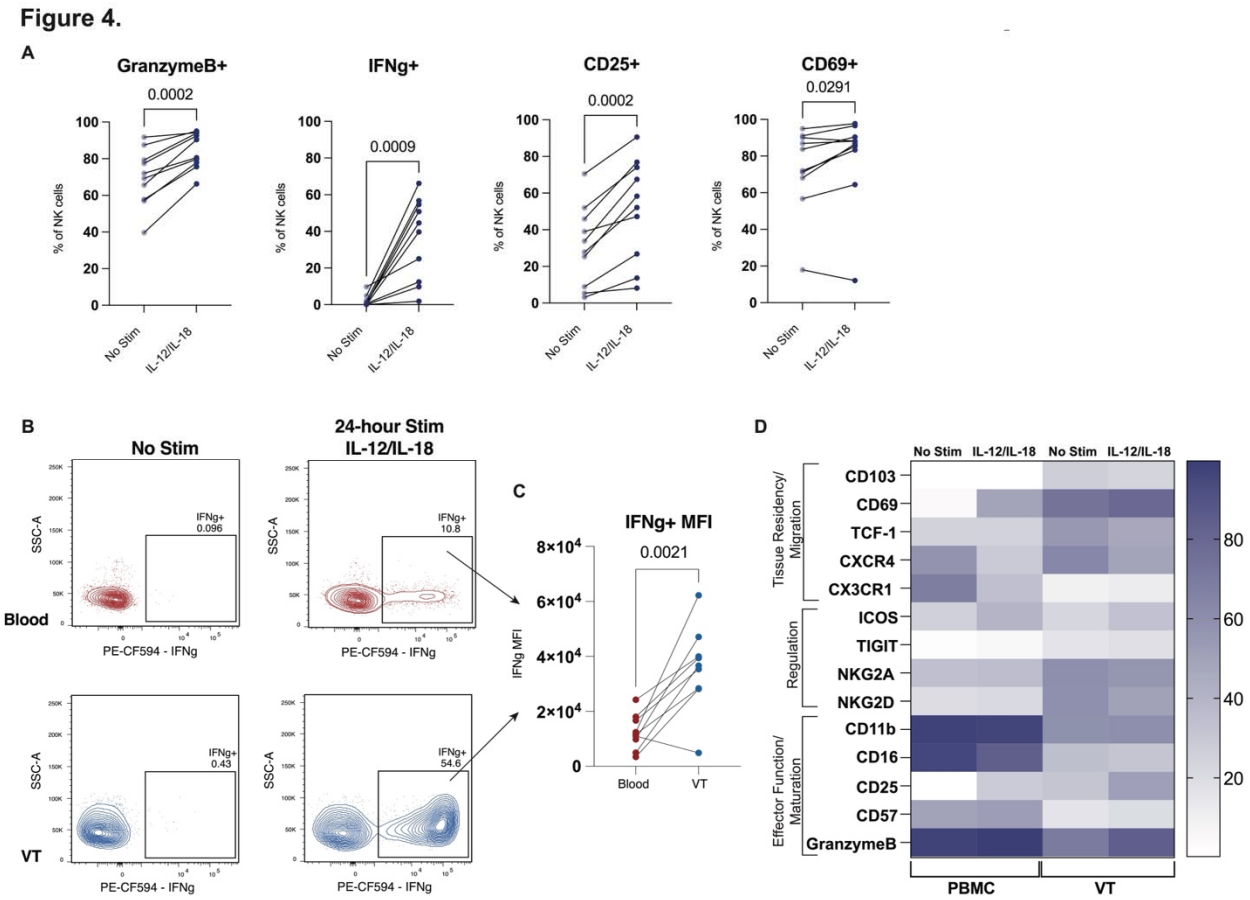

Figure 4. NK cells from vaginal tissue are able to produce an anti-pathogen effector response upon stimulation. Flow cytometry was performed on immune cells isolated from vaginal tissue (VT) or blood (PBMC) from healthy donors and stimulated ex vivo with 10ng IL-12 and 10ng IL-18 or with media alone for 24 hours. **A**) Graphs demonstrate frequencies of NK cells expressing markers of activation and effector function from media alone (n=10) or stimulation with IL-12/IL-18 (n=10). **B**) Example flow plot of NK cell expressing IFNg under stimulation or no stimulation conditions. **C**) Median fluorescent intensity was calculated from the IFNg+ population of NK cells after IL-12/IL-18 stimulation from blood (n=9) or VT (n=9) and graphed. **D**) Heat map displaying the mean frequencies of selected markers expressed on NK cells after IL-12/IL-18 stimulation or without stimulation conditions. Statistical analyses were performed using paired t test, p values listed.

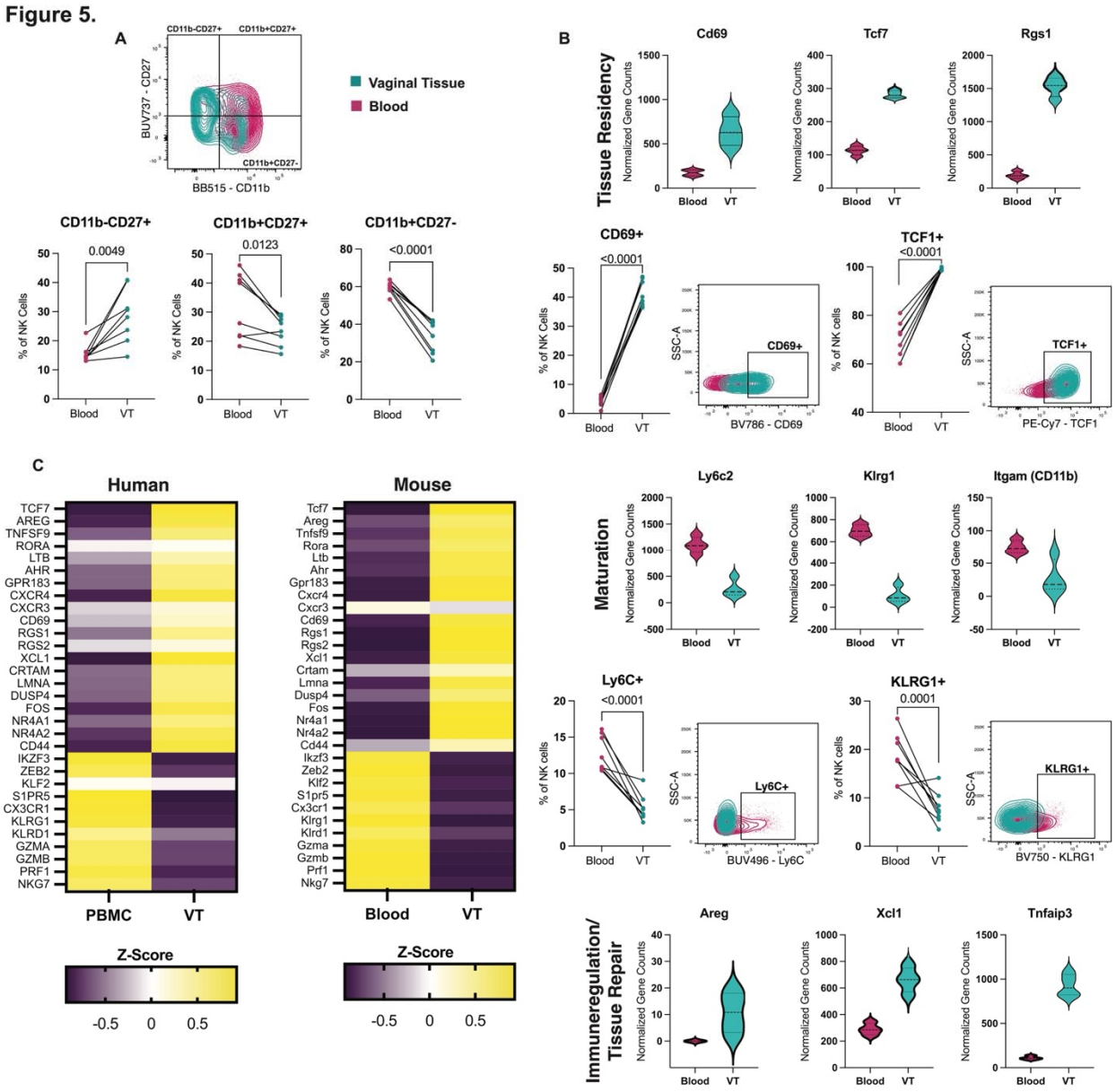

Figure 5. Mouse tissue NK cells compared to circulating NK cells show similarities to corresponding human NK cell subsets. Vaginal tissues and blood were harvested from uninfected C57BL/6 female mice. NK cells defined as Lymphocytes/SingleCells/Live/ CD45+/Ly6G-/CD19-/CD3-/NK1.1+. Bulk RNA sequencing was performed on sorted NK cells using SmartSeqV4 Ultra Low Input RNA Kit for Sequencing. Flow cytometry was performed on IV Label- NK cells. **A**) Paired graph showing NK cells gated on CD11b and CD27 subsets shown in example flow plot from blood (n=8) or VT (n=8). **B**) Violin plots showing normalized gene counts for selected genes and example flow plots with graphed frequencies from NK cells isolated from blood (left) or VT (right). NK cells expressing markers of tissue residency, maturation, and tissue-residency and immune regulation. RNA-seq data shows n=4 for blood and VT samples. Flow cytometry data shows n=8 for blood samples and VT

samples. Flow cytometry data are combined from two independent experiments. **C**) Heat map of calculated z-score for selected genes comparing circulating NK cells to tissue NK cells in both human (left) and mouse (right). Statistical analyses were performed using paired t test, with p values listed.

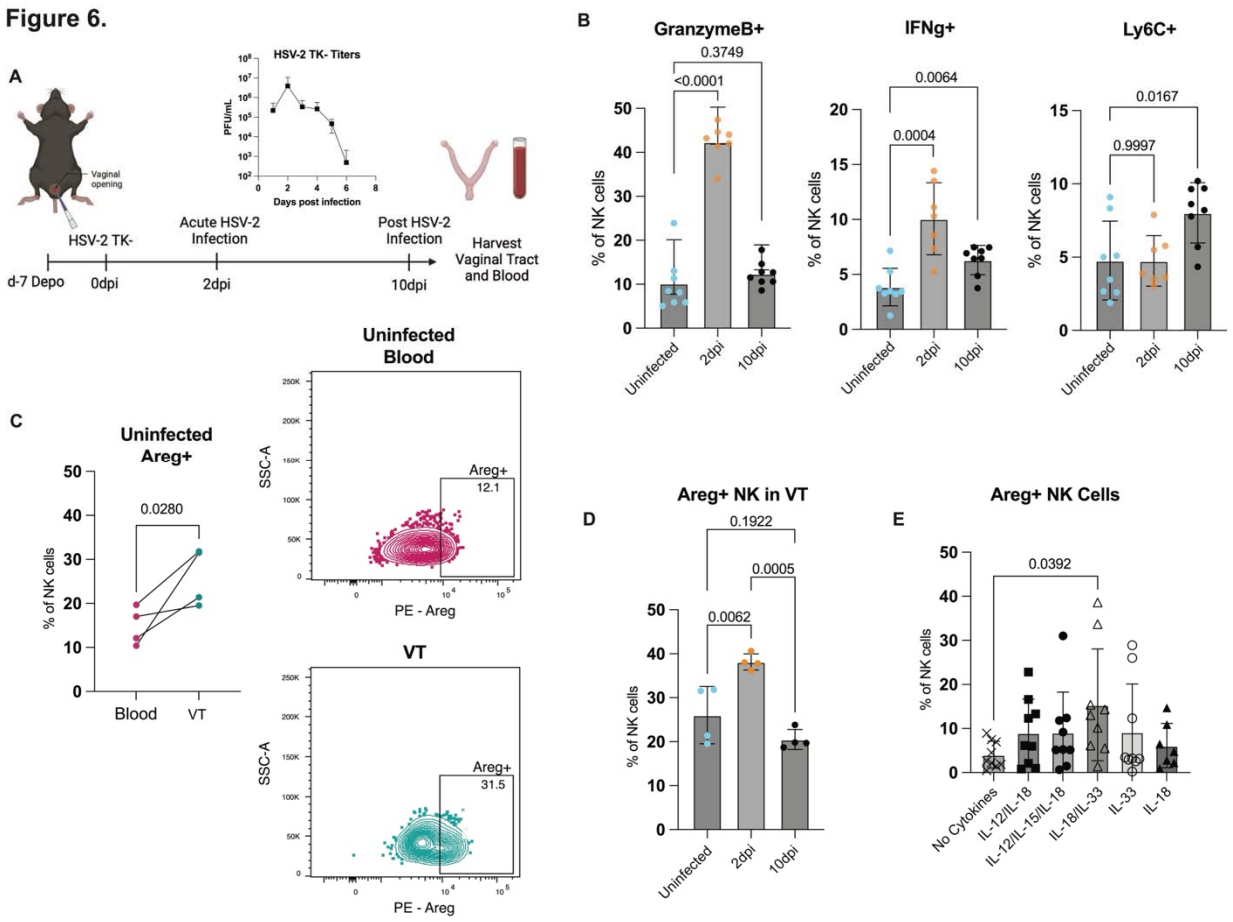

Figure 6. NK cells produce cytotoxic and tissue repair molecules during HSV-2 infection. C57BL/6 female mice were infected vaginally with $2x10^6$ PFU HSV-2 TK- and vaginal tissues and blood were harvested at 2 days post infection (dpi) and 10dpi and from uninfected mice. Flow cytometry was performed on NK cells gated on Lymphoctyes/ SingleCells/Live/ CD45+/Ly6G-/CD19-/CD3-/NK1.1+/IVLabel-. **A**) Experimental design demonstrating strategy for examining NK cells from vaginal tissue or blood at an acute infection time point (2dpi) and post infection time point (10dpi). Viral titers from vaginal washes after HSV-2 TK- infection demonstrate peak infectivity at 2 days post infection and viral clearance by 8 days post infection. **B**) NK cells were stimulated ex vivo with IL-12/IL-18 for 24 hours at 37 ºC to measure recall potential. Flow cytometry data indicating frequency of NK cells expressing cytotoxic molecule granzyme B, pro-inflammatory IFNg, and memory marker Ly6C, from uninfected mice (n=8), 2dpi (n=8) or 10dpi (n=8). **C**) Example flow plot and graphed frequencies of NK cells expressing Areg in uninfected mice comparing blood (n=4) to VT (n=4). **D**) Graphs showing the frequency of NK cells expressing Areg from VT across infection time points (n=4). **E**) Splenocytes isolated from naive C57BL/6 female mice were cultured in RP10 plus IL-2 for 24 hours and stimulated with combinations of IL-12, IL-15, IL-18, and IL-33 cytokines. Graph shows the frequency of NK cells expressing Areg under the different cytokine conditions (n=9). Data combined from three independent experiments. In **B** and **D**, data are presented as mean with SD, and statistical analysis used multiple

unpaired t-test, p values listed. Data are combined from two independent experiments. In **C**, statistical analysis was performed using paired t test, with p values listed. Representative data from two independent experiments. In **E**, data are presented as mean with SD and statistical analysis was performed using ordinary one-way ANOVA, p values listed.

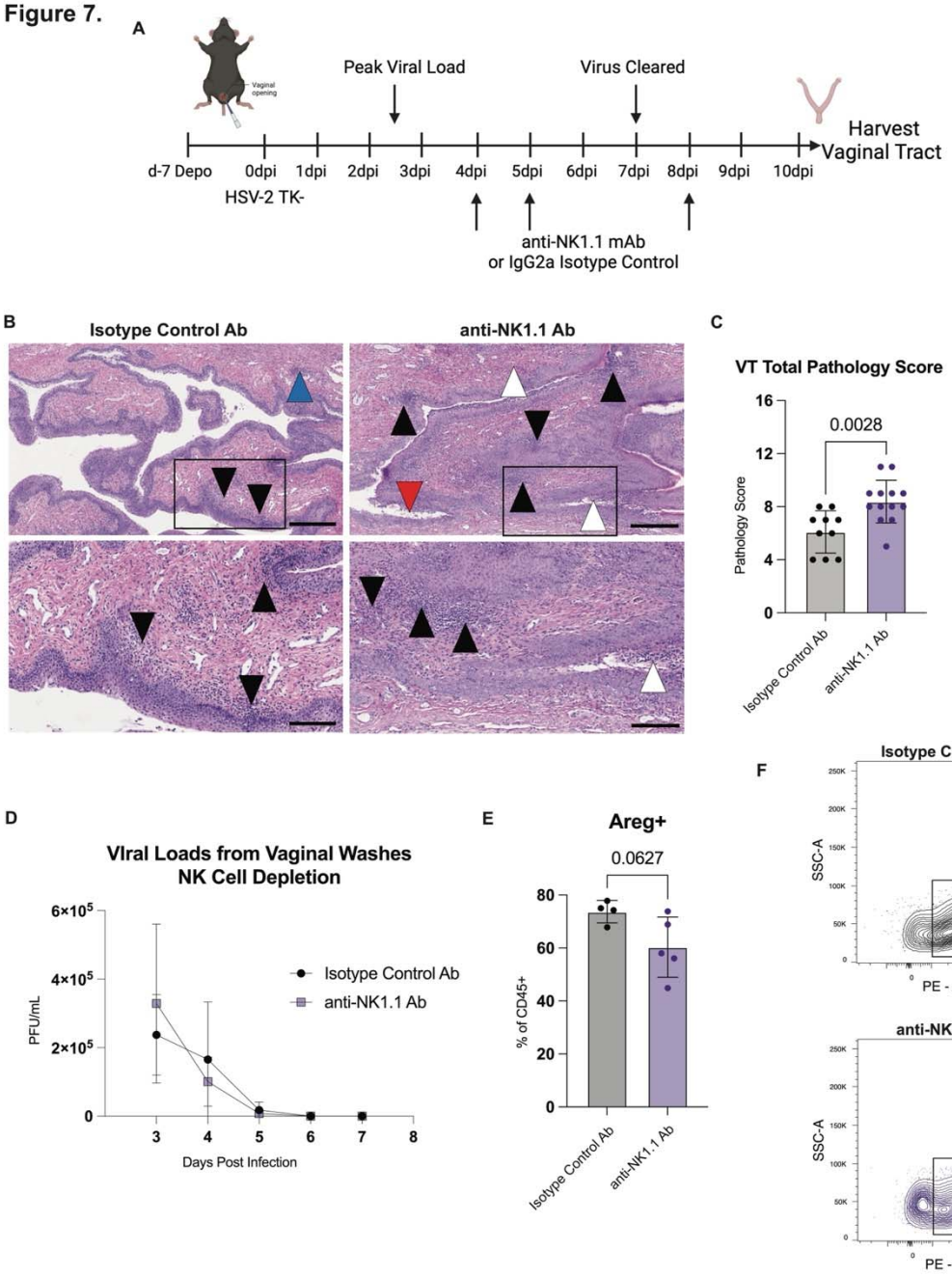

Figure 7. NK cell depletion after HSV-2 infection leads to increased tissue damage. A) Experimental model demonstrating mice were infected with $2x10^6$pfu HSV-2 TK- and administered 200ug of NK cell depleting antibody anti-NK1.1 or IgG2a isotype control antibody on days +4, +5, and +8 after infection. Vaginal tissues from mice were harvested on day +10 after infection for H&E staining or flow cytometry. **B**) Representative H&E images from an isotype control (left) and NK cell depleted (right) vaginal tissue. Arrowheads indicate lesions in the vaginal epithelium (white arrowhead), lamina propria (black arrowhead), muscularis (blue arrowhead) or lumen (red

arrowhead). Scale bar 500 uM (top), 100 uM (bottom). **C**) Total pathology scores from H&E images for isotype control (n=10) or NK cell depleted (n=13) groups. **D**) Viral loads from vaginal washes taken from mice daily after infection with HSV-2 TK-. Viral titers were calculated using plaque assays day +3 post infection before NK cell depletion and then daily until day +8 post infection when the virus was cleared (n=4 isotype control, n=4 anti-NK1.1). **E)** Frequency of Areg+ of CD45+ cells in mice treated with isotype control (n=4) or anti-NK1.1 (n=5). Cells were gated on TimeGate/Lymphocytes/SingleCells /CD45+Live /Areg+. **F**) Representative flow plot demonstrating Areg staining on CD45+Live cells. Data are combined from two independent experiments. In **C** and **E**, data are presented as mean with SD, and statistical analysis used unpaired t-test, p values listed.